







Article

New Perspectives for UAV-Based Modelling the Roman Gold Mining Infrastructure in NW Spain

Javier Fernández-Lozano ^{1,*}, Alberto González-Díez ¹, Gabriel Gutiérrez-Alonso ^{2,3}, Rosa M. Carrasco ⁴, Javier Pedraza ⁵, Jacinta García-Talegón ², Gaspar Alonso-Gavilán ², Juan Remondo ¹, Jaime Bonachea ¹ and Mario Morellón ¹

¹ Department of Earth Sciences and Physics of the Condensed Matter, Faculty of Sciences, University of Cantabria, Avenida de los Castros s/n, 39007 Santander, Spain; gonzalea@unican.es (A.G.-D.); juan.remondo@unican.es (J.R.); jaime.bonachea@unican.es (J.B.); mario.morellon@unican.es (M.M.)

² Department of Geology, Faculty of Sciences, University of Salamanca, Plaza de la Merced s/n, 38007 Salamanca, Spain; gabi@usal.es (G.G.-A.); talegon@usal.es (J.G.-T.); gavilan@usal.es (G.A.-G.)

³ Geology and Geography Department, Tomsk State University, Lenin Street, 36, Tomsk 634050, Russia

⁴ Department of Geological Engineering and Mining, Faculty of Environmental Sciences and Biochemistry, University of Castilla-La Mancha, Avenida Carlos III s/n, 45071 Toledo, Spain; rosa.carrasco@uclm.es

⁵ Department of Geodynamics, Stratigraphy and Paleontology, Faculty of Geological Science, Complutense University of Madrid, C/José Antonio Novais, 12, 28040 Madrid, Spain; javierp@ucm.es

* Correspondence: j.fernandezlozano@unican.es; Tel.: +34-942-201-512

Received: 5 September 2018; Accepted: 6 November 2018; Published: 9 November 2018



Abstract: This contribution discusses the potential of UAV-assisted (unmanned aerial vehicles) photogrammetry for the study and preservation of mining heritage sites using the example of Roman gold mining infrastructure in northwestern Spain. The study area represents the largest gold area in Roman times and comprises 7 mining elements of interest that characterize the most representative examples of such ancient works. UAV technology provides a non-invasive procedure valuable for the acquisition of digital information in remote, difficult to access areas or under the risk of destruction. The proposed approach is a cost-effective, robust and rapid method for image processing in remote areas where no traditional surveying technologies are available. It is based on a combination of data provided by aerial orthoimage and LiDAR (Light Detection and Ranging) to improve the accuracy of UAV derived data. The results provide high-resolution orthomosaic, DEMs and 3D textured models that aim for the documentation of ancient mining scenarios, providing high-resolution digital information that improves the identification, description and interpretation of mining elements such as the hydraulic infrastructure, the presence of open-cast mines which exemplifies the different exploitation methods, and settlements. However, beyond the scientific and technical information provided by the data, the 3D documentation of ancient mining scenarios is a powerful tool for an effective and wider public diffusion ensuring the visualization, preservation and awareness over the importance and conservation of world mining heritage sites.

Keywords: unmanned aerial vehicles (UAV); Roman gold mining; photogrammetry; mining; geoheritage

1. Introduction

Gold has extraordinary physical-chemical properties and represents one of the scarcest elements in nature. Average abundances in the Earth's crust vary from 0.001 to 0.006 ppm (g/t) [1]. The extremely bright and intense yellow color, together with its wide ductility makes gold a coveted mineral since antiquity [2]. The world's oldest gold manufactured objects, found in the Necropolis of Varna (Bulgaria) and dating back from the VI millennium BC, represents the earliest attempts of gold metallurgy [3]. Since then, gold acquired an increasing relevance in ancient southern Europe cultures [4]. Gold has

been also established as a standard of value and currency since the world's first coinage in Lydia (643–630 BC) [5]. However, significant advances in ore deposits prospection and exploitation did not occur until the onset of the New Age. The systematic exploitation of gold ore deposits may have started during the period of Roman domination in the Mediterranean. According to recent archaeological findings in the mining site of Pino del Oro (Zamora), Sánchez-Palencia et al. [6] suggest that the earliest prospection works in northwest Spain started during pre-roman times. The northwest Iberian Peninsula represents the largest Roman gold mining prospect in the world, with the Las Médulas world-class site as one of the most remarkable gold mines due to its important landscape transformation [7–9]. In this area, more than 93.5 billion m³ of Cenozoic sediments were removed by the Romans, recovering upon 5 t of gold [10]. Due to its archaeological and natural values, this site was declared a UNESCO World Heritage Centre in 1997, although recent works based on Airborne Laser Scanning Technology (ALS) suggests that it may not be the largest Roman goldmining site in terms of recovered gold quantities [11,12].

Roman gold mining works in northwest Spain were active from the 1st until the 3rd centuries AC. After that period, little gold mining-related information is known, with only minor documented exploitations during the Middle Ages and the Renaissance. Renewed interest in gold exploration emerged in the XXI century, which eventually led to the acquisition of several mining rights by Irish and Canadian mineral resources companies in northwest Iberia. This recent to present-day “gold rush” flourished due to the high potential for gold resources within Iberia and especially those found in the northwest. Nowadays, the implementation of LiDAR (Light Detection and Ranging) technology and UAVs has strongly simplified prospection works and mining management operations at mining sites [13]. However, the analysis and description of ancient mining works are of major importance when searching for evidence of ore-deposits [14]; especially relevant in other areas that were occupied by the Roman Empire, such as Britain, Romania, Greece or Turkey, where important resources may be still unexplored [15].

Beyond their mining, archaeological and scientific interest, Roman mining remains in northwest Spain constitute a good economic resource as well as a relevant touristic attraction in rural areas. However, the lack of any kind of preservation directives for this remarkable mining heritage remains—especially in non-profitable and remote areas located over 1600 m.a.s.l. altitude in mountainous areas—, with outstanding implications for the interpretation of the ancient mining landscapes, urges the need for digital preservation and public awareness. In the last few years, the interpretation of ancient goldmining infrastructure has been improved using ALS. High-resolution DEMs derived from ALS have provided reliable data for the morphological analysis of mining sites, supply canals and water reservoirs involved in the mining works [11,12,16,17]. However, ALS data are not always available, nor the resolution is often enough for an accurate and reliable interpretation of the archaeological remains. Moreover, processing of ALS point clouds can be a tedious and time-consuming task that requires a high computing capacity. Traditionally, aerial orthoimages have been used for a description of gold mining sites [18–20], but the images scale used commonly does not allow enough quality and resolution for the generation of 3D models. Unlike these aforementioned techniques, the recent growth and implementation of UAV-assisted photogrammetry have strongly contributed to a rapid and cost-effective method for mining exploration and research. Depending upon the dimensions and complexity of the mining site, UAVs provide a powerful tool for image capture in remote scenarios. For instance, large-scale mining sites can be rapidly surveyed using fixed-wing UAVs, while detailed surveying of small areas, characterized by a complex geometry and rough topography, can be performed using a more efficient rotatory wing UAVs [21,22]. Nowadays, UAVs have been implemented for topographic surveying of steep slopes and open-pit mines, calculations of ore stockpiles, monitoring dust particles after blasting and security management are starting to be of common use in the mining industry [23–26]. Additionally, the implementation of FLIR (Forward Looking Infrared Radiometer)-thermal and hyperspectral frame cameras have provided interesting

information for prospection works [27–29]. Other airborne sensors, such as magnetic, have also extensively contributed to a more detailed surveying of ore deposits and structural analysis [30].

Lately, new advances have been used in the archaeomining field to implement the reconstruction and study of ancient mining heritage remains. Documentation of archaeological sites have demonstrated the high capabilities and accuracy of orthomosaics and DEMs derived from UAVs in comparison to other sources of information such as a Terrestrial Laser Scanner (TLS) [31]. Special attention has been also paid for the preservation of cultural and geological heritage affected by mining activity [32,33]. However, the identification, description and modelling of the complex Roman mining infrastructure in northwest Spain using UAVs have received little attention [21,34].

The Teleno Mountain ranges, located in the southwestern province of León (NW Spain), represents a natural laboratory to test the application of UAV technology for the description and preservation of ancient goldmining infrastructure, comprising canals, water reservoirs and mines. The high concentration, dimensions, and reduced extent of the mining elements encouraged us to establish a rapid, high resolution and cost-effective UAV-approach based on ground control points acquisition from a combination of available aerial orthoimages and airborne LiDAR data from the Spanish “Plan Nacional de Ortofotografía Aérea” (PNOA). This method has been proven in the area as the choicest in previous works [11,34] and allows comparison of the different kinds of mining workings under the same circumstances. The results aimed at the accurate surveying of mining heritage remains in remote and mountainous areas where traditional surveying techniques cannot be performed effectively. The purpose of this article is to explore the potential of UAV-derived products (orthomosaics, DEMs and 3D textured models) for scientific research, public diffusion and preservation of ancient mining remain. From the dozens of possible study cases in the considered area, seven were chosen because of their representativeness. The seven models exemplified in this work cover the whole range of workings sizes and scales, all the exploitation systems, the different substrates and include all the diverse elements, mostly hydraulic, that are present in the region. The seven examples used also provide the opportunity to test the different methods of data acquisition using UAVs. We have tested and documented the convenience of automatic vs. manual flight plans for a data acquisition as a function of the model size and geometry, local topography, vegetation and weather conditions. Furthermore, the proposed approach for mining heritage reconstruction can be implemented in other ancient mining heritage scenarios across the world, especially where strong anthropic landscape transformation has occurred, and, more importantly, in abrupt, remote, inaccessible or unexplored regions [35,36].

2. Geology of Gold Deposits

A wide variety of natural gold deposits occurs in northwest Spain. The origin of these deposits is controlled by sedimentary and tectono-structural conditions, and they mostly comprise two main types: primary or endogenous and secondary or placer deposits [37]. Both types are represented in northwest Spain at the Teleno Range and its surroundings.

2.1. Primary Gold Deposits

Primary gold is found along the highest sectors of the Teleno and Cabrera Mountains. The area is part of the Variscan Deformation Belt, in the boundary of the so-called West Asturian-Leonese and Central Iberian Zones [38,39]. These deposits are associated with folded and faulted Ordovician rocks, although gold in Silurian limestones has also been reported to occur [40–42]. Geochemical data from the Eria River Valley showings have provided from 80 to 260 ppb and 30 ppb of gold in middle Ordovician slates and volcanic rocks, respectively [43]. A lesser amount of gold has been also described in the underlying Ordovician quartzites (4 ppb in Serie Los Cabos) [43].

The main mineralized showings are related to a wide conjugate fracture network filled with quartz-bearing from NE-SW to NW-SE trending veins and dikes [42,44]. These fault networks are interpreted as part of a stockwork like ore deposit caused by the deformation that folded and fractured

upper part of the crust. Additionally, saddle-reef type deposits have been identified in the area. They are characterized by the presence of large triangular volumes of white quartz filling the hinge of open folds, such as the Manzaneda anticline [42].

The origin of these quartz veins and dikes have been explained as related to a deep source of heat, probably associated with granitoid intrusion in the nearby Sanabria region. These magmatic bodies are responsible for the presence of meso- and hypothermal fluids silica and CO₂-rich fluids (200–400 °C). This is supported by the analysis of fluid inclusions, which suggest that the veins origin is related to multistage arsenopyrite, pyrite and iron oxides ore deposition [44].

Present-day prospection works performed in Paleozoic rocks have established an average gold grade of ca. 1.3 g/t, with strong variations associated to enriched disperse veins with grades that may reach over 10 g/t in the nearby Pino del Oro area [4].

2.2. Secondary or Placer Gold Deposits

Small gold particles are also concentrated in sedimentary deposits in northwest Spain (Figure 1a). Weathering and erosion affecting Paleozoic rocks facilitate the separation of the mineral particles from the quartz veins and its subsequent transport and deposition by the fluvial action of rivers and streams. During sedimentation, major gold concentrations are associated with rubefacted (iron-rich) Tertiary alluvial and fluvial deposits [41,45], whereas gold grades strongly vary within the sedimentary column [40]. Domergue and Hérail [8] also suggest that gold concentration follows a certain distribution, arguing a strong correlation between sediments with pebble grain-size facies and the amount of gold found in Cenozoic deposits. In addition, the highest gold concentrations are located close to the bed-rock sourcing the Cenozoic sediments and decreases towards the upper levels of the sedimentary succession.

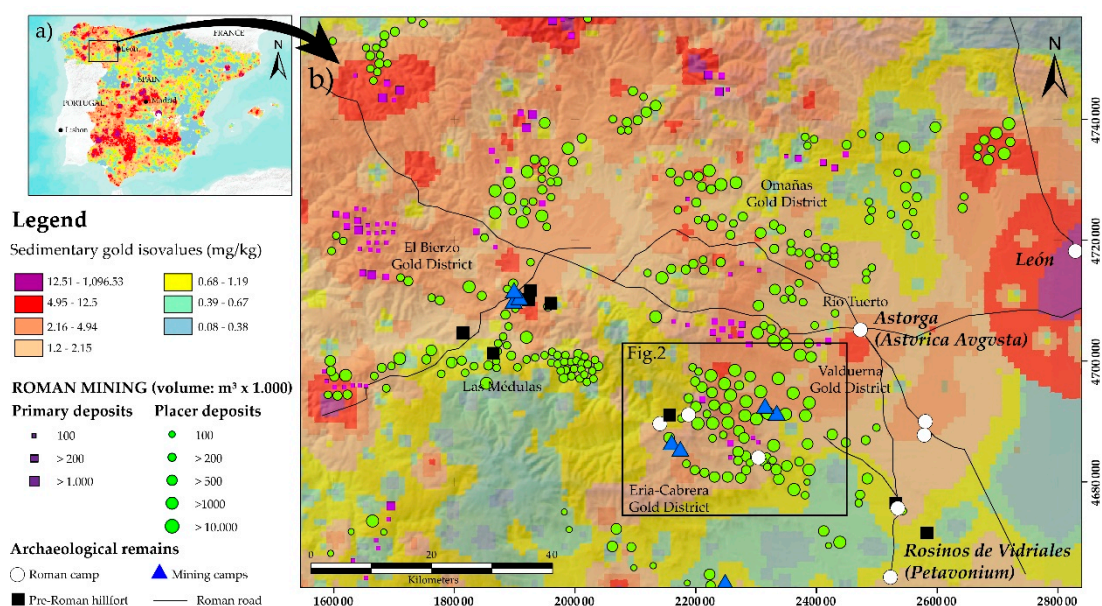


Figure 1. (a) Distribution of auriferous sedimentary deposits in Spain. (b) 1 km cell interpolation of sedimentary gold isovalues (mg/kg) in the studied region and its surroundings in northwest Spain and distribution of Roman gold mining works and related infrastructure. Data from the Spanish Geological Survey [46].

This type of gold deposits can also be found in Quaternary deposits. Fluvial terraces, that were exploited by the Romans, provide gold grades that vary from 31 mg/m³ to 115.8 mg/m³ in the Castrocontrigo area (see Figure 1b). In the nearby Valduerna valley, gold grades vary from 41.3 to 111 mg/m³, establishing a gold reserve of 5 to 6 t [40]. Similar values are observed in other Gold Districts such as Omañas, located further north of the study area. Another interesting fact is the

large-scale exploitation works carried out by the Romans in the glacial (till) deposits of the upper part of the valleys in the Teleno Mountains. Although the gold grades strongly vary in this type of sediments than in the previously described, they were also exploited during the Roman times [8,19].

To perform the gold extraction from sedimentary ore deposits, the Roman miners developed an intricate system of canals and water reservoirs. This hydraulic network is preserved in many sectors of the study area as shown below. The remains of the washing process of placer deposits are still recognized over the mining landscapes. It is represented by the accumulation of large volumes of waste material, locally-called *murias*, that comprises quartz and quartzite pebbles configuring grey rocky-patches over vegetated hillsides and valleys.

3. Roman Goldmining Infrastructure in Northwest Spain

Roman gold mining in northwest Spain comprises a series of sites or districts reported since the early 70 s. The first systematic studies were carried out at Las Médulas [7,47–49]. At the same time, geoarchaeological works initiated in the nearby Eria and Valduerna Districts based on traditional aerial image interpretation [8,18,19,50]. More recently, airborne laser technology (ALS or LiDAR) and UAVs were implemented for a re-evaluation of the prior investigations to shed light into new findings [11,12]. Other interesting vestiges of Roman gold mining in the northwest have been described in Las Omañas and Tuerto areas but aroused little interest due to the reduced dimensions and broad dispersion of the remains [51].

In the light of the new advances carried out in the province of León, investigations have focused on the identification, description and understanding of the complex infrastructure developed for the exploitation of gold from different perspectives: archaeological, historical, technical, geological-geomorphological and technological [9,12,21,45]. Overall, this study provided a good source of information that allows improving the knowledge over the transformation of mining landscapes and the implemented methodology for gold prospection and exploitation during the Roman period.

3.1. Hydraulic Infrastructure

The Roman hydraulic system consists of a large network of canals that exceeds more than 800 km only in the province of León, where a single canal runs through more than 140 km [50,52,53]. Reduced slopes characterize these canals (<1.2%), which frequently keep a standard size diameter of 1.20 to 1.50 m [40,47,52,54,55], with mean caudal of 0.2–0.7 m³/s—considering a sheet of water upon 0.4–0.6 m—[50].

There are two different types of canals: supply and derivation. On the one hand, supply canals connect rivers, streams and springs from the valleys with the main mining sites. Over 2000 m.a.s.l., in the Teleno Mountains, water was also captured from snow melting. On the other hand, derivation canals were used for water discharge when overflow problems may occur or even when mining areas needed further supply. It is common that canals were built on rock, aiming at their preservation (mainly in the more friable slates). In addition, canals constructed over sedimentary rocks have also been identified in the study area [11].

Another hydraulic element devised by the Roman engineers was the water reservoirs or tanks. There, water was collected and subsequently distributed through a system of canals that supplied the main exploitation sites. The shape and dimensions of these reservoirs strongly depended on the water requirements and the availability of water to maintain the exploitations running.

3.2. Mining Activity

Mining activity comprised both subsurface and surface exploitation during the Roman period. While primary gold deposits were mostly exploited through galleries and trenches, there was a wide range of mining methods implemented for gold extraction in secondary placer deposits. Thus, depending on the thickness and extension of the ore deposits the typology may vary. For example, secondary deposits, Las Médulas-type, consisting on a thick pile of tertiary red conglomerates show

remains of a series of excavated galleries and pits in the sedimentary succession. Tanks located in the upper mountainous areas supplied water to the opened pits and galleries. This skeleton-like structure served to weaken the whole mountain, dismantling millions of cubic meters in a single operation. The method, called *Ruina montium* by Pliny the Elder, has been described too for >30 m thick tertiary and quaternary deposits in nearby areas of La Cabrera and Ancares [56]. The explanation for this large-scale exploitation is found in the presence of major grades found at the bottom of the sedimentary succession, close to the bedrock. However, most of the secondary deposits comprise shallow deposits instead. They are located on the mountain fronts covering large areas due to the erosion and weathering of the bedrock. Exploitations carried out in thin sedimentary bodies display trenches, comb-like open-cast mines and other superficial features affected by ground-slucing. Water supplied by canals from water reservoirs located in the mountains served to wash the sedimentary beds, reducing the waste material to large accumulations of *murias* or tailing deposits.

4. Materials and Methods

In order to analyze and describe this infrastructure, we have performed a series of UAV flights to carry out a photogrammetric reconstruction. The aerial photogrammetric survey of the Roman gold mining infrastructure consisted of the acquisition of aerial images from 7 highly representative elements of the northwest mining captured across the Teleno area (Figure 2). Due to the geographic constraints and feature characteristics (i.e., strong topography, rocky outcrops and ledges, size, the geometry of the outcrop, security and maneuvering possibilities), different flight modes (manual vs automatic) were implemented in order to provide the best results. The main surveyed elements represented well-preserved examples of the following Roman mining remains:

- Two different examples of open-cast mine: deep and shallow mining representatives
- Tailing deposits
- Hydraulic infrastructure comprising: a rock passageway for transferring water from one valley to another and a stepped network of tanks for water storage
- A water supply canal system
- Roman mining camp

All the above features provide a good overview of the different hydraulic remains and mining techniques used by the Romans for the exploitation of gold deposits, and present in other nearby mining sectors, such as Bierzo-Las Médulas, Omañas or Valduerna (Figure 1). The concentration, small-scale dimensions, and reduced extension of these mining heritage elements make the study area a suitable laboratory for the acquisition of 3D digital information. Unlike traditional aerial digital photogrammetry, where the camera model and its positions are required, Structure from Motion (SfM) obtains this information from computer vision procedures (using algorithms such as SIFT [57]) to estimate camera positions from the used images, which aims at the reconstruction of 3D structures from 2D images [58–61] (Figure 3). Thus, at least a minimum overlap of three images are necessary for an appropriate bundle adjustment result.

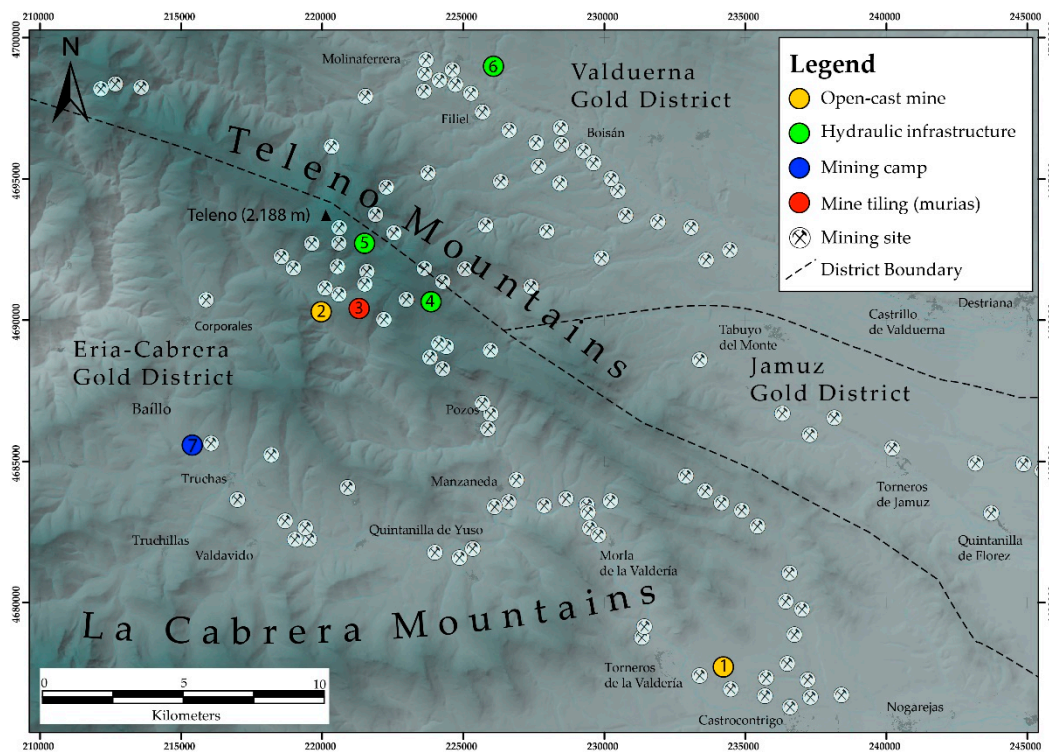


Figure 2. Distribution of Roman mining sites in the Teleno Mountains and its surroundings and location of study elements comprising open-cast mines and tailing deposits, hydraulic infrastructure, and a mining camp. Numbers: 1, Model 1; 2, Model 2; 3, Model 3; 4, Model 4; 5, Model 5; 6, Model 6 and 7, Model 7.

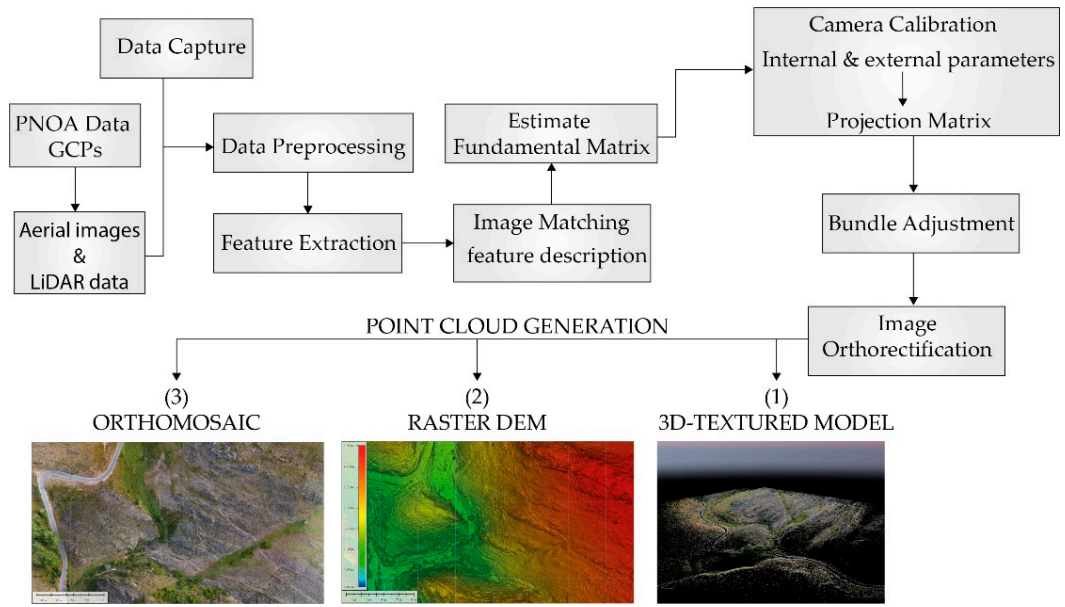


Figure 3. Structure from Motion (SfM) process of image implementation and derived data. Processing of images comprises computer vision feature extraction and image matching before the initialization of matrix estimations and camera parameters calibration necessary for the bundle adjustment. The final processes consist of the generation of dense point clouds from which a 3D-texture, a DEM and an image orthomosaic are obtained respectively.

Data Acquisition and Processing

The data acquisition was performed using an electric Lipo-battery DJI Phantom 4 quadcopter-UAV with 30 min hovering time (Figure 4). The UAV included a 12.4 Megapixel camera model FC330_3.6_4000x3000 (DJI, Shenzhen, China) with a spherical lens and 94° field of vision, which reduces distortion upon 36% in comparison with a fish-eye lens, the Pix4D camera calibration module (École Polytechnique Fédérale de Lausanne (EPFL), Lausanne, Switzerland) was used to reduce the emergent distortion, following a two-step camera calibration method. This method is commonly used for accurate camera calibration estimation [62–65]. The camera CMOS sensor 1/2.3" comprised a lens with a focal length of 22 mm (equivalent to a 35 mm format) attached to a gimbal, which improved the camera calibration process by reducing discrepancies during the determination of orientation parameters [66]. In addition, due to the strong orography and changing weather conditions of the mountainous region, manual flight was performed around different elements, especially in those areas where these conditions limited the flight security. The image acquisition was planned using the IOS application Pix4D capture, which provides semi-automatic control of the flights. This application gives different options to control the speed and side- and end-lap. Flight speed was limited between 2 and 5 m/s depending on wind conditions. The flying set-up, comprising of a number of images, the projection of the pixel size onto the ground plane (GSD), surface, flying mode and flying height was recorded for later analysis. The overlap between images was configured in two modes: Image acquisition was performed using a distance-based capture during manual flight, whereas time interval capture was used for automatic flights. Both were set using the Pix4D capture application. Drone images were subsequently processed in Pix4D Mapper Software V.4.3.27 (École Polytechnique Fédérale de Lausanne (EPFL), Lausanne, Switzerland) for PC.



Figure 4. Quadricopter DJI Phantom 4 employed for surveying the mining remains.

The existing relationship between image and real coordinates was estimated for the camera calibration (Figure 3). Calibration consisted of establishing the internal orientation elements such as focal length and distortions. This process was performed using the Pix4D® Camera Calibration Module for DJI cameras, following SfM algorithms, which includes an analysis of the accuracy of the processing results. Because a single camera was used, the intrinsic camera parameters were maintained during processing.

External orientation was determined from 6 to 12 control points that were obtained using a non-traditional approach, due to the stepped topography and difficult access to certain zones.

Therefore, traditional topographic surveying, based in Real Time Kinematics-GPS, was replaced by measurements obtained from a digital photogrammetric model [67], which was generated from the PNOA project. The PNOA project is focused on the acquisition of 25 to 50 cm resolution orthoimages and DEMs from a digital photogrammetric treatment of aerial images captured by airplanes equipped with high-resolution position devices onto the Spanish territory, every 2–3 years [68]. This project also includes a LiDAR flight used for the model validation. The aerotriangulation of PNOA was performed for large areas; in this case, 5284 images distributed through 112 flight lines were used to obtain orthoimages with a pixel size below 25 cm. Their global accuracy was measured using 158 control points (Ground Control Points-GCP and Check Points-ChP): 29 GCP and 129 ChP with RMS-GCP (m): $X = 0.031$; $Y = 0.034$; $Z = 0.038$ and RMS-CHP (m): $X = 0.182$; $Y = 0.174$; $Z = 0.219$ [68].

Following the methodology suggested in previous studies [69], planimetric and altimetric values of control points from the PNOA project were used for georeferencing and validation of UAV images. Some of them were obtained from the aerotriangulation of the PNOA, while others from the LiDAR point clouds. Therefore, geolocation errors were significantly controlled.

Finally, the reconstruction of the 3D structure was achieved following the traditional bundle adjustment. It consists of the reconstruction of matching points through the 3D calculated coordinates. At a later stage, point extraction was computed for the acquisition of a densified point cloud, which was subsequently used for the generation of a triangulated irregular network necessary for the reconstruction of a DEM. A high-resolution orthomosaic was generated from the combination of image mosaics and georeferenced DEM, interpolated from a high-density point cloud. Thus, the final photorealistic model was generated by blending textures of objects derived from the images.

5. Results

The modelling of ancient mining heritage elements in remote areas results in a challenging task. Irregular topography and changing weather conditions play an important role, during the definition of the flying conditions, in mountainous areas, which hampered the feature marks visibility. However, other factors may influence these conditions too. For instance, the orography makes the maneuverability of the operations difficult to avoid accidents. Besides, the need to reduce the possible shadows that could occur due to the spatial relationships between the relief and sun position. In addition, to control the effect of light and differences in shadow direction, the flights were performed at dawn and sunset. This methodology improved the image resolution since SfM depends on pixel patterns for accurate identification of objects. Further details on accuracy and resolution methods implemented in the 3D mapping of mining heritage elements can be found in [11,34].

Another important factor is the design of the images overlapping. The difficulty to capture a suitable geometry controls the image overlap during the flights. Thus, forcing the implementation of manual or automatic flying modes according to the flight needs of each area (Figure 5). The accuracy of the point clouds was achieved by increasing image convergence (80% front overlap and 70% side overlap). To provide better results and reduce redundancies, the camera sensor was inclined 45° during the process of image acquisition, following previous experiences in 3D modelling carried out by Strecha et al. [62]. These authors argued that oblique images highly improve the processing results during the computing of optimization and orientation parameters. This is especially indicated for mountain areas characterized by strong topographic variations.

Modelling conditions for each site is presented in Table 1. Besides the number of images, surface, flying model and flying height, the raw GSD of the images was also included. The latter does not represent the resolution of the images in the final model, but the potential of those in order to obtain subsequent image analysis.

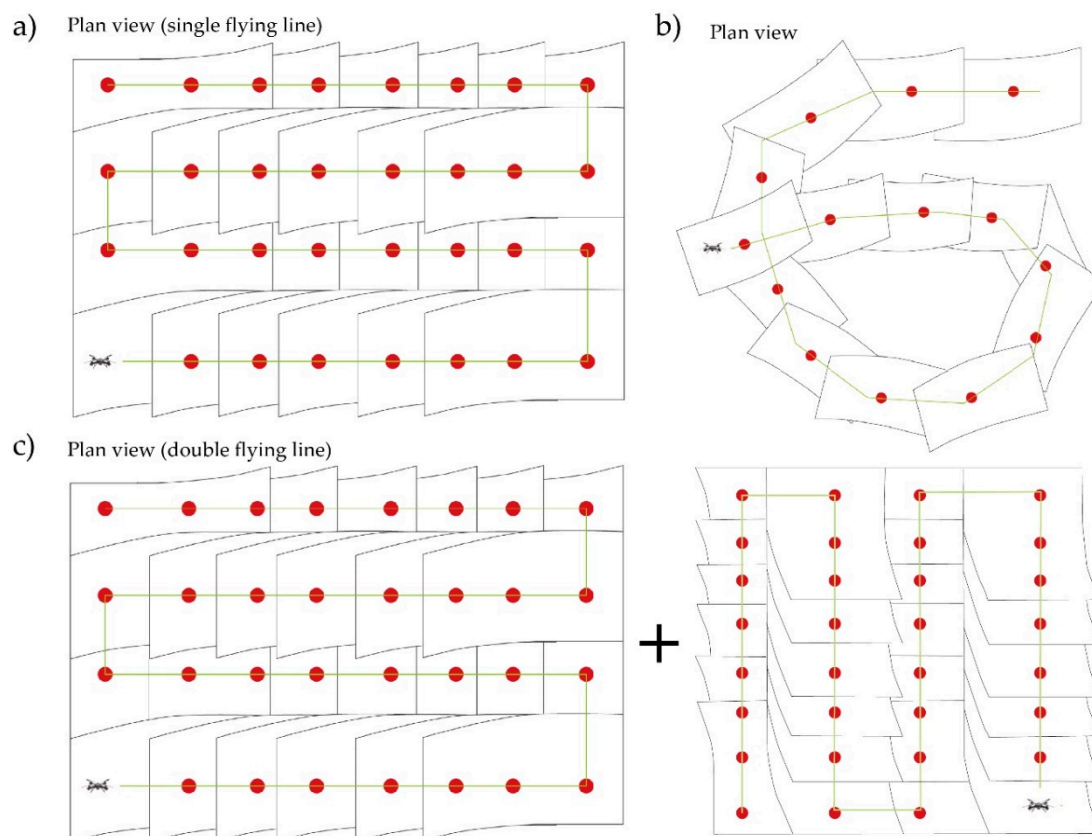


Figure 5. Flying modes implemented for mapping mining sites presented in this work. (a) Automatic flying mode and a single flying line: Model 1; (b) Manual flight: Model 3, 4 and 7; (c) automatic grid and double flying line: Models 2, 5 and 6. Red dots locate the image photocenters and black lines represent the image marks.

Table 1. Modeling conditions and principal flight information.

Model	Images	GSD (m)	Surface (ha)	Flying Mode	Height (m)
Model 1	270	0.0305	32.33	Rectangular grid	50
Model 2	283	0.0477	11.75	Rectangular grid	50
Model 3	325	0.0489	16.15	Manual	Vary
Model 4	536	0.0180	17.01	Manual	Vary
Model 5	372	0.0462	14.64	Rectangular grid	50
Model 6	423	0.0480	26.06	Rectangular grid	50
Model 7	63	0.1314	27.28	Manual	Vary

Table 2 shows the GCP and ChP accuracy data calculated for each model according to the methodology proposed by González-Díez [69]. None of the models provided a positional uncertainty of the geomorphic 3D vectors over 1 m. However, models 1 and 6 give steamily high values of uncertainty close to that limit. A possible reason for such a difference comes out from two types of uncertainties. The main limitation is provided by the difficulty to identify the marks of the control points on the PNOA photogrammetric model, which is strongly influenced by the input quality of both sets of images (PNOA and UAV images), which strongly depends in the stepped and shady topography and presence of dense vegetation cover. The second limitation was associated with the influence of the consumer grade GPS integrated into the UAV necessary for positioning the rest of points from the images. Therefore, in order to control this possible deviation, a comparison between PNOA orthoimages and UAV-derived images through Global Mapper GIS (Blue Marble Geographics

V.19) was carried out, ensuring the proper matching of the features and minimum deviation of the measurements, within the global accuracy mentioned above.

Table 2. Ground Control Points and Ground Check Points accuracy data. * Model global accuracy according to González-Díez [69].

Model	RMS-GCP X (m)	RMS-GCP Y (m)	RMS-GCP Z (m)	RMS-ChP X (m)	RMS-ChP Y (m)	RMS-ChP Z (m)	Model Global Accuracy (m) *	GCP	ChP
Model 1	0.401	0.635	0.151	0.351	0.693	0.537	0.944	5	3
Model 2	0.061	0.052	0.115	0.086	0.012	0.21	0.227	5	3
Model 3	0.101	0.189	0.035	0.161	0.628	0.201	0.679	4	3
Model 4	0.226	0.156	0.27	0.163	0.174	0.161	0.288	9	3
Model 5	0.006	0.114	0.068	0.046	0.116	0.163	0.205	5	3
Model 6	0.108	0.083	0.077	0.212	0.06	0.939	0.964	6	3
Model 7	0.131	0.088	0.413	0.319	0.119	0.111	0.358	4	3

A wide variety of representative mining examples were digitally recorded and reconstructed (Figure 5). A set of data consisting of an orthomosaic, a Digital Surface Model (DSM) and a 3D texture model was acquired for each mining feature. Models allowed an accurate and reliable calculation of volumes and surfaces for description of the Roman infrastructure, whereas 3D textures provide also useful information for its interpretation and visualization. 3D models are available in Supplementary Materials (Figures S1–S7).

5.1. Open-Cast Mining

Two well-preserved open-cast mines were studied (Figure 2). They comprise different examples of mining exploitation methods.

5.1.1. Model 1

Model 1 consists of a shallow open-cast mine. The products consist of an orthomosaic and DEM (geotiff extent), as well as a 3D textured model (3D-pdf). The accuracy of GCPs is shown in Table 2. CHPs global accuracy was 0.94 m. Strong differences in X, Y and Z were caused to some of the limitations explained in the methods section above. Due to the broad extension and good flight conditions (i.e., flat topography) of the outcrop two automatic flights 22 and 18 min long were taken, during which a set of 270 (100% calibrated) images were obtained. The extent of the modelling element consists of a large area. Hence, to reduce the large number of images, the flight was taken in a single flying line (Figure 5a). The total surface covered a rectangular grid upon 32.3 ha, surveyed at 50 m height. The 3D texture model generated had a Ground Sampling Distance (GSD) upon 0.3 m (Model 1, Table 1). The reconstruction shows a series of convergent canals ending into a washing canal, also known in the literature as *agogae* (Figure 6a). The 3D reconstruction shows a type of comb-like structure representative of shallow exploitations in secondary deposits (Miocene red conglomerates) occupying large extents [18,20]. Water supplied by canals was used to wash the sedimentary deposits, dismantling the entire auriferous sedimentary body. The convergent structures are formed by accumulations of quartzite boulders and pebbles extracted from the conglomerates, leading to tailing deposits called *urias*.



Figure 6. Oblique aerial images of the study sectors: (a) comb-like open-cast mine at Castrocontrigo (Model 1); (b) Deep open-cast mine (Model 2); (c) *Muriyas* deposits supporting a water reservoir (Model 3); (d) rock tunnel (Model 4); (e) water reservoirs (Model 5); (f) water supply canal (Model 6) and (g) a mining camp (Model 7).

5.1.2. Model 2

Model 2 is a characteristic remain of a deep open-cast mine. Like in the previous model, the final product consisted of an orthomosaic (geotiff), a DEM (geotiff) and a 3D texture (3D-pdf). However, this model showed small differences in GCPs accuracy with a global accuracy of CHP upon 0.22 m (Table 2). The flight took 22 min and the mosaic was completed with 283 images covering a total surface of 11.7 ha, although 92% of the images were calibrated. Images were captured using an automatic time-interval capture mode (Figure 5c). The strong mine height differences obliged to perform a double line flight in order to increase coverage, which improved the final modelling result. However, the observed reduction in the number of calibrated images could be due to the turbulences occurred during flight performance. Like in the previous model, the flight was performed in automatic mode using a rectangular grid, due to the clearance topographic conditions and small dimensions of the area. The model comprised a small mine sector where the irrigation system directly connects with a deep trench (≈ 50 m), and a tailing deposit at the bottom (Figure 6b). The exploitation was performed washing over the rubefacted quaternary hillside sediments.

5.2. Tailing Deposits (Model 3)

Model 3 consists of an orthomosaic (geotiff extent) and a 3D texture model (3D-pdf). There are subtle differences in RMS between X-Y and Z, although the global accuracy provided by the CHP was 0.67 m. Due to the presence of a high vegetation cover and the complex geometry of the mining remains, the feature was flown in manual mode (see Figure 2 for location and Figure 5b). It took about 20 min to capture 325 pictures varying flying altitude (< 20 m high) with 100% of images calibrated. Images were taken using distance-based capture to provide enough coverage of the mining element.

Tailing deposits, also called in northwest Spain *murias*, represent the waste material accumulated during the exploitation works. They are characteristic of Roman mining works performed in Tertiary and Quaternary auriferous deposits. In general, they extend over large surface areas allowing the identification of Roman works by the presence over the local vegetation of grey pebbly patches. Figure 4c shows a good example that served for the protection and stability of a water reservoir located over the tailing deposit. As shown in the image, a supply canal connects with the tank, providing a source of water for the nearby mining sector. The water reservoir dimensions reach upon 4887 m². According to Pliny the Elder in his *Naturalis Historia* these reservoirs may reach 2 to 3 m deep [52]. Therefore, assuming a 2.5 m deep structure, the total volume of this tank may reach 12,217 m³.

5.3. Hydraulic Infrastructure (Models 4, 5 and 6)

A broad network of canals and water reservoirs extending from the bottom of the valleys to the upper sectors of the Teleno Mountains constitutes the hydraulic infrastructure of this Roman mining site (Figure 6c–e).

5.3.1. Model 4

Model 4 consisted of a 3D textured model (3D-pdf). Little variations were observed in GCP RMS accuracy and the ChP global accuracy was 0.28 m (Table 2). Due to the strong topography of the area and the short space for safe maneuvering of the UAV, together with the presence of nooks and crannies that reduced visibility and control of the UAV, flight was performed using a manual flight (Figure 5b) of 22 min 536 images were captured using a distance-based capture (5 m interval). To improve the modelling results, the camera was oriented at 45° and the flight was run at different altitude taking into account the safety needs, although maintaining always as close to the mining remains as possible, to obtain a GSD up to 0.018 m.

This model corresponds to a rock tunnel. This type of features is among the most astonishing structures (Figure 6d). They are excavated in hard quartzite and allowed the derivation of water from

one valley to another. These structures were used as shortcuts to reduce high slopes. In most cases, the slope was reduced by reinforced masonry that also aimed at the preservation of the supply canals.

5.3.2. Model 5

The reconstruction of Roman water reservoirs (similar to the one mentioned in Model 3) provided a high-resolution orthomosaic and DEM (geotiff extent, Figure 7a,b) and a 3D textured model.

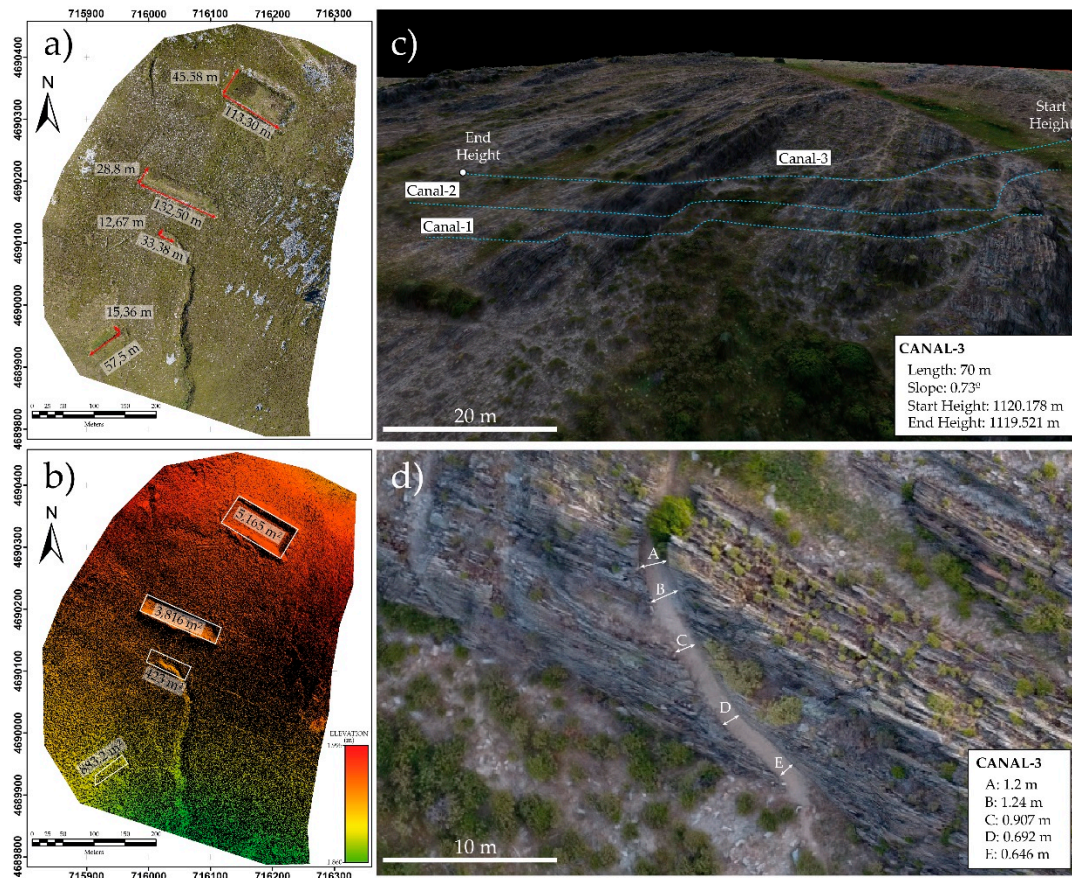


Figure 7. (a) Orthomosaic and (b) DSM from water reservoirs also called *maseras* (Model 5). 3D model of hydraulic infrastructure (Model 6). (c) Three supply canals excavated in slates. Water flow from right to left. Measurements of dimensions and characteristics of canal 3. (d) Differences in diameter measured in canal 3 along a curved section.

Model 5 provided the best accuracies with GCP-RMS between 0.006 and 0.11 m and a ChP global accuracy of 0.20 m. Despite the mining remains were located at a high altitude in the most remote area, the visibility conditions were good and there were no obstacles around that may compromise the safety of the flight. Thus, a 22 min automatic flight, based on time-interval capture and two flying lines (Figure 5c), was carried out over a rectangular grid (8 × 10 lines) at 50 m height. The total surface reached 14.63 ha for the reconstruction of a final image. During the flight, 372 images were taken with 100% calibrated images. Some radio interference problems were observed due to the nearby presence of a present-day military base in the area.

Model 5 comprised a series of stepped water reservoirs. They are considered as one of the most important elements on the hydraulic infrastructure developed by the Romans in the area. They served for the collection of water and snow. Figure 6e shows three Roman water reservoirs in the Teleno Mountains [20,52]. They are popularly called *maseras*. These stepped reservoirs may have been used for the accumulation of snow deriving snowmelt water from one another that was subsequently distributed according to the mining needs. From top to bottom, the main measurements are 5165 m²,

3816 m², 432 m² and 883.2 m². As shown above, assuming a 2.5 m depth, the total volumes are about 10,330 m³, 9540 m³, 1080 m³ and 2207.5 m³, respectively (Figure 6a,b).

5.3.3. Model 6

A DSM and orthoimages (geotiff extent) were obtained for the description and interpretation of the hydraulic system. Additionally, a 3D-textured model (3D-pdf) was generated for public diffusion and analysis of the infrastructure. The model was based in a set of 423 images obtained from two automatic flights that took in total 35 min long. Due to the good visibility and flat topography of the area the altitude of the flight was set to 50 m covering a large surface of 26.06 ha. Images were acquired using an automatic time-interval capture using a two flying lines approach (Figure 5c), and all the images were calibrated. The GCPs accuracy was relatively high compared with other models (Table 2), although the ChP global accuracy was one of the highest (0.96 m).

Model 6 configures another good example of the hydraulic infrastructure, represented by canals excavated in slate rock (Figure 6f). Canals run over large distances leading to a total network that extends over 800 km within the León Province (NW Spain) [50,52,53]. The study example was followed over 70 m length. It comprises three stepped canals with a mean slope of 0.6°–0.8°. Measurements carried out on canal-3 over the DSM model points to a water direction descending from right to left in Figure 6c. In addition, the diameter of the canal box varies along the line. Thus, major diameters are found in the curves, whereas reduced dimensions are observed in the straight parts (Figure 7d). These size differences would serve to avoid the damage of the canals and the loss of water due to the hydraulic force.

5.4. Mining Camps (Model 7)

Model 7 consisted of a 3D textured model (3D-pdf extent) based on 63 images, all of them calibrated. The flight was performed manually varying the height and following a circular trajectory around the structure (Figure 5b). Images were acquired following a distance-based capture mode (every 15 m) due to the extent covered by the element and the nearby presence of high vegetation. The flight surface covered 27.28 ha and the final GSD reached 0.13 m. Despite the GCP-RMS was high in Y (see Table 2), the ChP global accuracy reached 0.35 m.

This type of mining settlements is distributed in the nearby mining sectors of the Teleno Mountains. They are characterized by the presence of deep trenches and a bulls-eye geometry (Figure 6g). The rounded geometry led several authors to coin the name *coronas* (crowns) for this type of structures [18,50]. A combined defensive and mining utility have been invoked since they relate to the main hydraulic infrastructure through a network of canals [17,18,70,71]. Archaeological remains described in the nearby crown of Quintanilla relate these elements to Roman mining camps dated in the year 15 A.D. [72]. They were probably occupied to ensure the control and adequate development of mining and maintenance tasks related to the mining infrastructure in the area.

6. Discussion

The rapid and accurate methodology developed for the documentation of Roman mining infrastructure preserved in the Teleno Mountains highlights the potential of UAV-assisted photogrammetry in the reconstruction of remote mining landscapes inaccessible through traditional surveying techniques (Figure 8). The wide distribution of remains impedes the visualization and suggests the need for digital reproductions that aim at their study and preservation. Traditional aerial imagery and LiDAR point clouds do not provide enough resolution for the identification, description and 3D reproduction of heritage sites [73]. Likewise, processing LiDAR point clouds involve a large number of computer resources with high costs. However, in the last few years, the implementation of new photogrammetric approaches, such as SfM, in UAVs has considerably reduced costs, simplifying data acquisition and processing.

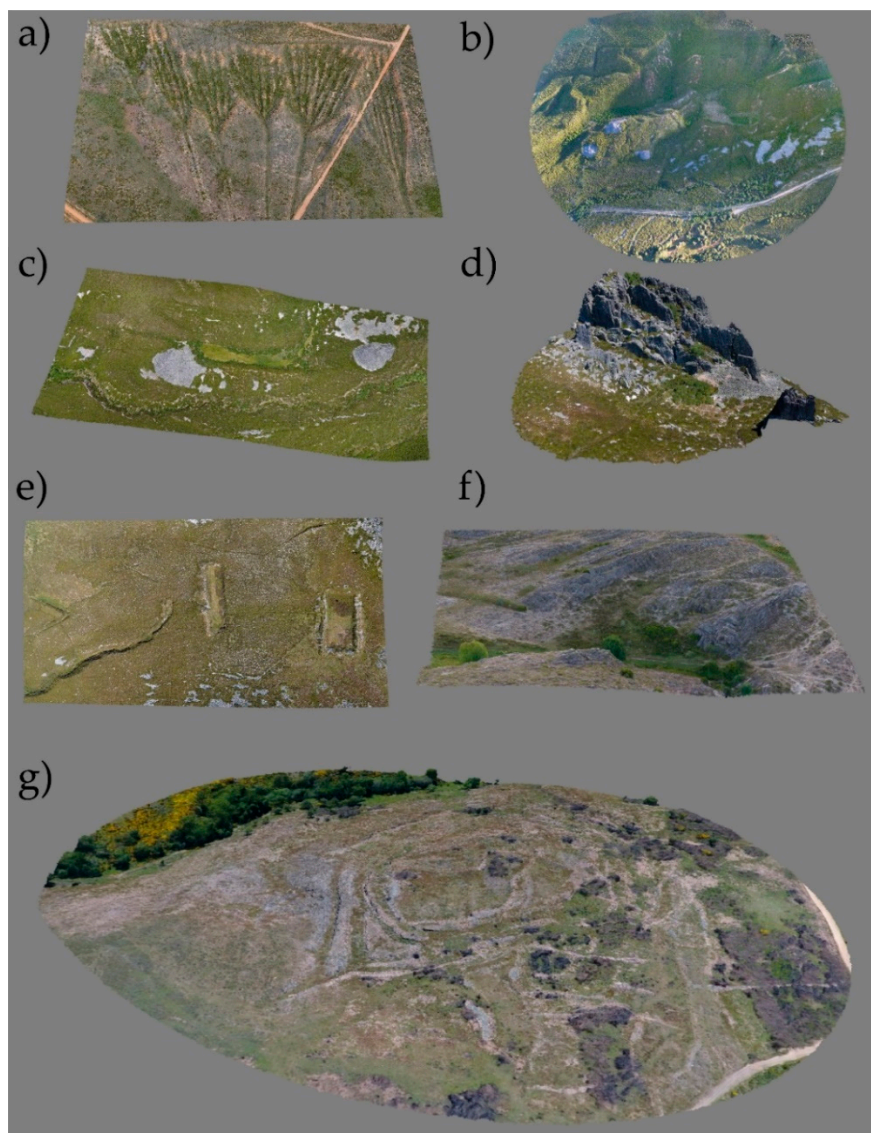


Figure 8. 3D texture models: (a) shallow open-cast mine (Model 1); (b) deep open-cast mine (Model 2); (c) tailing deposits (Model 3); (d) rock tunnel (Model 4); (e) stepped water reservoirs (Model 5); (f) supply canals (Model 6) and (g) mining camp (Model 7). Models available in Supplementary Materials (Figures S1–S7).

SfM has strongly contributed to reduce complex and time-consuming processing tasks providing a rapid and accurate method for the generation of orthomosaics, high-resolution DEMs and 3D texture maps [74,75]. This digital information provides accurate information for topographic reconstruction, reducing time and costs, and increasing safety for each mining operation [76–78].

Besides all these benefits, the acquisition of accurate and reliable data improves mining evaluation and managing tasks, which in turn provides better results for the mining industry.

In the last few years, the use of UAVs for the rapid evaluation of mining sectors is largely extended. Although most of the studies focus on present-day operations, recent research has shown the versatility of UAV-assisted photogrammetry for the location and description of ancient mining sites [21,31]. Historical mines have provided important information about the location and type of ore deposits. Invaluable information, essential for the development of new prospection tasks. In fact, many present-day prospection works initiate at these historical sites. This is the case of the auriferous deposits located in northwest Spain, originally started in pre-roman times [6]. In this area, the location of canals and water reservoirs aim at the identification of ancient mining sites.

Its relevance and dimensions can help to locate the most prolific deposits according to the dimensions of the infrastructure. Thus, large-scale auriferous sedimentary deposits required large amounts of water supplied by canals and water reservoirs.

However, beyond the significant amount of scientific and mining information provided by the Roman infrastructure preserved, mining landscapes possess a great heritage value for society [17,79,80]. There are many world mining examples that have been used for diffusion of cultural heritage by UNESCO, such as the Rammelsberg mines (Germany), Iwami Ginzan Silver Mine (Japan), Guanajuato Historic Mines (México), Wieliczka and Bochnia Royal Salt Mines (Poland), Flint Mines at Spiennes (Belgium), Almaden and Rio Tinto (Spain), Big Pit coal mines (Wales). Among them, Las Médulas represent one of the best examples of cultural heritage musealization. However, in the last decade, 3D documentation works have led to a broad field of possibilities for mining heritage diffusion and preservation still unexplored in the Roman Gold Mining infrastructure. 3D models improve visualization and allow virtual tours that create a sensation of immersion, creating a great impact on the public (Figure 8). This is especially important in areas where mining heritage is inaccessible or prone to destruction. Virtual musealization of archaeological sites provides numerous benefits for rural areas or regions under development, by adding value to their heritage and foresting public awareness about its importance and conservation [81,82]. Thus, these techniques allow us to put in values such as historic-industrial heritage.

As shown above, UAV-assisted photogrammetry provides a powerful approach for the study and conservation of historical remains. The method is rapid and cost-effective, providing reliable and high-resolution information. It is worth notice the remarkable value of UAV-assisted technology for the mining heritage assessment and preservation and its important implications for the evaluation and documentation of similar world mining heritage remains.

7. Conclusions

As shown above, the implementation of UAV-assisted photogrammetry for the 3D digital recording of mining heritage remains contributes to a better identification and description of the mining features and its scientific interpretation and evaluation. The possibility to acquire high-resolution 3D texture volumes, able to visualize from different perspectives and light conditions, improves the identification and assessment of each mining element. Moreover, the high resolution of the orthomosaics and DEMs allow accurate measurements for volume and length calculations. This is especially important in remote and difficult to access areas, such as the Teleno Mountains, where traditional methods lack enough resolution for an accurate and rapid analysis of the mining landscape. The Teleno Mountains and surrounding areas represent one of the most prolific auriferous regions in western Europe during the Roman period. The large amount of material remobilized together with its extension provides a remarkable imprint of the mining activity carried out over more than two centuries on the landscape. However, despite some efforts made by the Spanish Administration to provide a public overview of the goldmining works in the famous area of Las Medulas, a well-known World Heritage Centre declared in 1997 by UNESCO, most of the Roman infrastructure remains are still inaccessible or already lost in the mountains. The high topography of the area and the widespread vegetation hide most of the mining elements, comprising a complex hydraulic system of canals and water reservoirs, an impressive network of deep and shallow exploitations with farfetched geometries and shapes, and a good representation of mining settlements. Altogether, it represents an outstanding transformation of the landscape with a worth scientific and public interest still unexplored. Therefore, UAVs are a cost-effective and rapid method to provide digital information in this type of areas. This technology also aims at the public diffusion and awareness over ancient mining heritage elements, especially in areas under the risk of destruction or disappearance, which lacks any preservation directives. In light of the above, the characterization of ancient mining landscapes using UAVs highlights the potential for the three-dimensional reconstruction of heritage elements, which can be easily implemented in other important world mining sites.

Supplementary Materials: The following are available online at <http://www.mdpi.com/2075-163X/8/11/518/s1>. Figure S1: Roman shallow mine, Figure S2: Deep Roman mine, Figure S3: *Murias*, Figure S4: Rock tunnel, Figure S5: Water reservoirs, Figure S6: Supply canals, Figure S7: Mining settlement.

Author Contributions: All authors have contributed substantially to the work reported. J.F.-L. is a UAV pilot and operator certified by the Spanish Agency of Aerial Security. Fieldwork was carried out in cooperation with UCLM, UCM and USAL Universities. Processing and writing were performed by UC researchers.

Funding: This research was funded by the Spanish Ministry of Science, Innovation and Universities (CGL2016-78380-P) and the Russian Federation project: Origin, metallogeny, climatic effects, and cyclical large igneous provinces (14.Y26.31.0012).

Acknowledgments: We are indebted for the inestimable suggestions and advice provided by four anonymous reviewers who have significantly contributed to improve the quality of this manuscript. We would like to thank the Castrocalbón Archaeological and Ethnographic Museum (León) and the support provided by the Castrocontrigo and Truchas Majors and their municipal corporations.

Conflicts of Interest: The authors declare no conflict of interest. The funders had no role in the design of the study; in the collection, analyses, or interpretation of data; in the writing of the manuscript, and in the decision to publish the results.

References

1. Enghag, P. *Encyclopedia of the Elements: Technical Data. History, Processing, Applications*; Wiley-VCH: Weinheim, Germany, 2004; p. 1309, ISBN 978-3-527-30666-4.
2. García-Moreno, O.; Aguirre-Palafox, L.E.; Álvarez, W.; Hawley, W. A Little Big History of Iberian Gold. *J. Big Hist.* **2017**, *1*, 40–58. [[CrossRef](#)]
3. Leusch, V.; Armbruster, B.; Pernicka, E.; Slavčev, V. On the invention of gold metallurgy: The gold objects from the Varna I cemetery (Bulgaria)—Technological consequence and inventive creativity. *Camb. Archaeol. J.* **2015**, *25*, 353–376. [[CrossRef](#)]
4. Rivas y de Hoyos, A.; Barrios-Sánchez, S.; Lozano-Fernández, R.P. *Pepitas de oro Españolas*; Cuadernos del Museo Geominero; Museo Geominero: Madrid, Spain, 2017; Volume 23, p. 182, ISBN 978-84-9138-048-1.
5. Macdonald, E. *Handbook of Gold Exploration and Evaluation*; Elsevier: Cambridge, UK, 2007; p. 630, ISBN 978-1-84569-175-2.
6. Sánchez-Palencia, F.J.; Perona, D.R.; Ortega, A.B. Geoarqueología del oro en la Zona minera de Pino del Oro (Zamora). *Mélanges de la Casa de Velázquez* **2018**, *1*, 63–87. [[CrossRef](#)]
7. Sánchez-Palencia, F.J.S.P.; Fernández-Posse, M.D.; Fernández-Manzano, J.; Álvarez-González, Y.; López-González, L.F. La zona arqueológica de las Médulas (1988–89). *Archivo Español de Arqueología* **1990**, *63*, 249–264.
8. Domergue, C.; Hérial, G. Conditions de gisement et exploitation antique à Las Médulas (León, Espagne). *Aquitania Suppl.* **1999**, *9*, 93–116.
9. Sánchez-Palencia, F.J.S.P.; Fernández-Posse, M.D.; Fernández, M.J.; Orejas, A.; Pérez-García, L.C.; Sastre, I. Las Médulas (León), un paisaje cultural patrimonio de la humanidad. *Trabajos de Prehistoria* **2000**, *57*, 195–208. [[CrossRef](#)]
10. Pérez-García, L.C.; Sánchez-Palencia, F.J. El yacimiento aurífero de Las Médulas: Situación y geología. In *Las Médulas (León). Un Paisaje Cultural en la «Asturia Augustana»*; Sánchez-Palencia, F.J., Ed.; Instituto Leonés de Cultura: León, Spain, 2000; pp. 144–188, ISBN 84-89470-87-1.
11. Fernández-Lozano, J.; Gutiérrez-Alonso, G.; Fernández-Morán, M.Á. Using airborne LiDAR sensing technology and aerial orthoimages to unravel roman water supply systems and gold works in NW Spain (Eria valley, León). *J. Archaeol. Sci.* **2015**, *53*, 356–373. [[CrossRef](#)]
12. Matías, R.; Llamas, B. Use of LIDAR and photointerpretation to map the water supply at the Las Murias-Los Tallares Roman gold mine (Castrocontrigo, León, Spain). *Archaeol. Prospect.* **2018**, *25*, 59–69. [[CrossRef](#)]
13. Pukanska, K.; Bartos, K.; Sabova, J. Comparison of Survey Results of the Surface Quarry Spišské Tomášovce by the Use of Photogrammetry and Terrestrial Laser Scanning. *Inžynieria Mineralna* **2014**, *15*, 47–54.
14. Davis, R.A.; Welty, A.T.; Borrego, J.; Morales, J.A.; Pendon, J.G.; Ryan, J.G. Rio Tinto estuary (Spain): 5000 years of pollution. *Environ. Geol.* **2000**, *39*, 1107–1116. [[CrossRef](#)]
15. Lehrberger, G. The Gold Deposits of Europe. In *Prehistoric Gold in Europe*; Monteani, G., Northover, J., Eds.; Springer: Dordrecht, The Netherlands, 1995; pp. 115–144, ISBN 978-94-015-1292-3.

16. Fonte, J.; Pires, H.; Gonçalves-Seco, L.; Matias, R.; Lima, A. Archaeological research of ancient mining landscapes in Galicia (Spain) using Airborne Laser Scanning data. In *Atas do Simpósio Internacional Paisagens Mineiras Antigas na Europa Occidental*; Câmara Municipal: Boticas, Portugal, 2014; pp. 198–199.
17. Currás-Refojos, B.; Romero, D.; Sánchez-Palencia, F.J.; Pecharromán, J.L.; Reher, G.; Alonso, F. Minería de oro antigua en la cuenca del río Negro (Zamora). In *Minería Romana en Zonas Interfronterizas de Castilla y León y Portugal (Asturia y NE de Lusitania)*; Sánchez-Palencia, J.F., Ed.; Documento Pahis; Junta de Castilla y León, Consejería de cultura y Turismo: León, Spain, 2012; pp. 217–229, ISBN 978-8469715796.
18. Fernández-Posse, M.D.; Sánchez-Palencia, F.J. *La Corona y el Castro de Corporales II: Campaña de 1983 y prospecciones en la Valderia y la Cabrera (León)*; Ministerio de Cultura, Dirección General de Bellas Artes y Archivos, Junta de Castilla y León, Consejería de Educación y Cultura: León, Spain, 1988; 262p, ISBN 978-84-5058-267-3.
19. Sánchez-Palencia, F.J. Prospecciones en las explotaciones auríferas del NO de España (Cuencas de los ríos Eria y Cabrera y Sierra del Teleno). *Not. Arq. Hisp.* **1980**, *8*, 214–289.
20. Sáenz-Ridruejo, J.; Vélez-González, C. *Contribución al Estudio de la Minería Primitiva del oro en el Noroeste de España*; Ediciones Atlas: Madrid, Spain, 1974; p. 190, ISBN 978-8440009586.
21. Fernández-Lozano, J.; Gutiérrez-Alonso, G. Aplicaciones geológicas de los drones. *Rev. Soc. Geol. Esp.* **2016**, *29*, 89–105.
22. Lee, S.; Choi, Y. Reviews of unmanned aerial vehicle (drone) technology trends and its applications in the mining industry. *Geosyst. Eng.* **2016**, *19*, 197–204. [[CrossRef](#)]
23. McLeod, T.; Samson, C.; Labrie, M.; Shehata, K.; Mah, J.; Lai, P.; Wang, L.; Elder, J.H. Using video acquired from an unmanned aerial vehicle (UAV) to measure fracture orientation in an open-pit mine. *Geomatica* **2013**, *67*, 173–180. [[CrossRef](#)]
24. Alvarado, M.; Gonzalez, F.; Fletcher, A.; Doshi, A. Towards the development of a low-cost airborne sensing system to monitor dust particles after blasting at open-pit mine sites. *Sensors* **2015**, *15*, 19667–19687. [[CrossRef](#)] [[PubMed](#)]
25. Lee, S.; Choi, Y. Topographic survey at small-scale open-pit mines using a popular rotary-wing unmanned aerial vehicle (drone). *Tunnel Undergr. Space* **2015**, *25*, 462–469. [[CrossRef](#)]
26. Martin, P.G.; Payton, O.D.; Fardoulis, J.S.; Richards, D.A.; Scott, T.B. The use of unmanned aerial systems for the mapping of legacy uranium mines. *J. Environ. Radioact.* **2015**, *143*, 135–140. [[CrossRef](#)] [[PubMed](#)]
27. Honkavaara, E.; Eskelinen, M.A.; Pölonen, I.; Saari, H.; Ojanen, H.; Mannila, R.; Holmlund, C.; Hakala, T.; Litkey, P.; Rosnell, T.; et al. Remote sensing of 3-D geometry and surface moisture of a peat production area using hyperspectral frame cameras in visible to short-wave infrared spectral ranges onboard a small unmanned airborne vehicle (UAV). *IEEE Trans. Geosci. Remote Sens.* **2016**, *54*, 5440–5454. [[CrossRef](#)]
28. Li, F.; Yang, W.; Liu, X.; Sun, G.; Liu, J. Using high-resolution UAV-borne thermal infrared imagery to detect coal fires in Majiliang mine, Datong coalfield, Northern China. *Remote Sens. Lett.* **2018**, *9*, 71–80. [[CrossRef](#)]
29. Ashley, S. Searching for land mines. *Mech. Eng.* **1996**, *118*, 62.
30. Eck, C.; Imbach, B. Aerial magnetic sensing with an UAV helicopter. *Int. Arch. Photogramm. Remote Sens. Spat. Inf. Sci.* **2011**, *38*, 81–85. [[CrossRef](#)]
31. Eisenbeiss, H.; Zhang, L. Comparison of DSMs generated from mini UAV imagery and terrestrial laser scanner in a cultural heritage application. *Int. Arch. Photogramm. Remote Sens. Spat. Inf. Sci.* **2006**, *36*, 90–96.
32. Pacina, J.; Kopecký, J.; Bedrníková, L.; Handrychová, B.; Svarcová, M.; Holá, M.; Pončíková, E. Information system for preserving culture heritage in areas affected by heavy industry and mining. In Proceedings of the EGU General Assembly Conference, Vienna, Austria, 27 April–2 May 2014; Volume 16.
33. Fernández-Lozano, J.; Gutiérrez-Alonso, G. The Alejico Carboniferous Forest: A 3D-terrestrial and UAV-assisted photogrammetric model for geologic heritage preservation. *Geoheritage* **2017**, *9*, 163–173. [[CrossRef](#)]
34. Fernández-Lozano, J.; Gutiérrez-Alonso, G. Improving archaeological prospection using localized UAVs assisted photogrammetry: An example from the Roman Gold District of the Eria River Valley (NW Spain). *J. Archaeol. Sci. Rep.* **2016**, *5*, 509–520. [[CrossRef](#)]
35. Tripcevich, N.; Vaughn, K.J. *Mining and Quarrying in the Ancient Andes*; Springer: Berlin, Germany, 2013; p. 386, ISBN 978-1461451990.
36. Ramage, A.; Craddock, P.T.; Cowell, M.R. *King Croesus' Gold: Excavations at Sardis and the History of Gold Refining*; British Museum Press: London, UK, 2000; Volume 11, p. 272, ISBN 9780674503700.

37. Boyle, R.W. *The Geochemistry of Gold and Its Deposits*; Bulletin/Geological Survey 280; Energy, Mines and Resources Canada: Geological Survey of Canada: Ottawa, ON, Canada, 1979; p. 584, ISBN 978-0660017693.
38. Spiering, E.D.; Pevida, L.R.; Maldonado, C.; González, S.; García, J.; Varela, A.; Arias, D.; Martín-Izard, A. The gold belts of western Asturias and Galicia (NW Spain). *J. Geochem. Explor.* **2000**, *71*, 89–101. [[CrossRef](#)]
39. Boixet, LL. Prospección de yacimientos auríferos en la Península Ibérica. *Tierra Tecnol.* **2015**, *48*, 3–8.
40. Pérez-García, L.C. Los sedimentos auríferos del NO de la Cuenca del Duero (Provincia de León, España) y su prospección. Tesis inédita, Universidad de Oviedo, Oviedo, Spain, 1977.
41. Hérail, G. *Géomorphologie et géologie de l'or détritique. Piémonts et bassins intramontagneux du Nord-Ouest de l'Espagne*; Éditions du CNRS, Centre de Toulouse, Sciences de la Terre; CNRS: Paris, France, 1984; p. 450, ISBN 978-2-222-03562-6.
42. Fernández-Lozano, J. Estudio geológico preliminar de un sector del cierre periclinal del Sinclinorio de Truchas (León): El anticlinal de Manzaneda. *Geogaceta* **2012**, *52*, 17–20.
43. Dixon-Porter, H.; Morán, B.A. Mineralizaciones de oro del noroeste de España. In *Recursos Minerales de España*; García-Guinea, J., Martínez-Frías, J., Eds.; Consejo Superior de Investigaciones Científicas, CSIC: Madrid, Spain, 1992; pp. 849–860, ISBN 84-00-07263-4.
44. Gómez-Fernández, F.; Vindel, E.; Martín-Crespo, T.; Sánchez, V.; Clavijo, E.G.; Matías, R. The Llamas de Cabrera gold district, a new discovery in the Variscan basement of northwest Spain: A fluid inclusion and stable isotope study. *Ore Geol. Rev.* **2012**, *46*, 68–82. [[CrossRef](#)]
45. Pérez-García, L.C.; Sánchez-Palencia, F.J.; Torres-Ruiz, J. Tertiary and Quaternary alluvial gold deposits of Northwest Spain and Roman mining (NW of Duero and Bierzo Basins). *J. Geochem. Explor.* **2000**, *71*, 225–240. [[CrossRef](#)]
46. IGME. Atlas Geoquímico de España. Instituto Geológico y Minero de España, 2012. Available online: <http://mapas.igme.es/Servicios/default.aspx> (accessed on 20 August 2018).
47. Lewis, P.R.; Jones, G.D.B. Roman gold-mining in north-west Spain. *J. Roman Stud.* **1970**, *60*, 169–185. [[CrossRef](#)]
48. Jones, R.F.J.; Bird, D.G. Roman gold-mining in north-west Spain, II: Workings on the Rio Duerna. *J. Roman Stud.* **1972**, *62*, 59–74. [[CrossRef](#)]
49. Domergue, C. De l'utilisation de l'eau pour le transport des matériaux: Le cas des mines romaines de Las Médulas (province de León, Espagne). In *L'eau: Usages, Risques et Représentations dans le Sud-Ouest de la Gaule et le Nord de la Péninsule Ibérique, de la fin de l'Âge du Fer à l'Antiquité Tardive (Ile saC-VIespC)*; Bost, J.P., Ed.; Aquitania: Talence, France, 2012; p. 21, ISBN 2-910763-24-2.
50. Matías, R. El agua en la ingeniería de la explotación minera de Las Médulas (León-España). *Lancia Rev. Prehistoria Arqueología Hist. Antigua Noroeste Peninsular* **2006**, *7*, 17–112.
51. Gutiérrez, R.B.G. Las explotaciones auríferas romanas del río de las Huelgas y su influencia en la transformación del paisaje (el ejemplo de Veguelina de Cepeda, León). *Cuadernos Investig. Geogr.* **1999**, *25*, 111–124. [[CrossRef](#)]
52. Sánchez-Palencia Ramos, F.J.; Pérez García, L.C. Las Médulas y la minería del oro romana en la Astvria Avgustana. Las Médulas (León). In *Las Médulas (León). Un Paisaje Cultural en la «Asturia Augustana»*; Sánchez-Palencia, F.J., Ed.; Instituto Leonés de Cultura: León, Spain, 2000; pp. 137–226, ISBN 84-89470-87-1.
53. Sastre, I.; Sánchez-Palencia, F.J. La red hidráulica de las minas de oro hispanas: Aspectos jurídicos, administrativos y políticos. *Arch. Esp. Arqueol.* **2002**, *75*, 215–233. [[CrossRef](#)]
54. López, D.G. *Las Médulas*; Ed. Nebrija: León, Spain, 1980; p. 159, ISBN 84-391-4011-8.
55. Pérez-García, L.C. Métodos de prospección de oro en diferentes depósitos aluvionares en España. In *Actas del Congreso Gisements Alluviaux d'or*; ORSTOM: La Paz, Bolivia, 1991; pp. 325–355.
56. Fernández-Lozano, J.; Andrés-Bercianos, R. Movimientos en masa naturales o inducidos: Nuevas aportaciones al estudio de inestabilidad de laderas en la provincia de León. *Geogaceta* **2018**, *62*, 1–4.
57. Lingua, A.; Marenchino, D.; Nex, F. Performance analysis of the SIFT operator for automatic feature extraction and matching in photogrammetric applications. *Sensors* **2009**, *9*, 3745–3766. [[CrossRef](#)] [[PubMed](#)]
58. Westoby, M.; Brasington, J.; Glasser, N.F.; Hambrey, M.J.; Reynolds, J.M. Structure-from-Motion photogrammetry: A novel, low-cost tool for geomorphological applications. *Geomorphology* **2012**, *179*, 300–314. [[CrossRef](#)]

59. Turner, D.; Lucieer, A.; Watson, C. An automated technique for generating georectified mosaics from ultra-high resolution unmanned aerial vehicle (UAV) imagery, based on structure from motion (SfM) point clouds. *Remote Sens.* **2012**, *4*, 1392–1410. [[CrossRef](#)]
60. Yi, G. Survey of Structure from Motion. In Proceedings of the IEEE International Conference on Cloud Computing and Internet of Things (CCIOT), Changchun, China, 13–14 December 2014; pp. 72–76.
61. Micheletti, N.; Chandler, J.H.; Lane, S.N. Structure from Motion (SfM) Photogrammetry. *Geomorphological Tech. Br. Soc. Geomorphol.* **2015**, *2*, 1–12.
62. Strecha, C.; Von Hansen, W.; Van Gool, L.; Fua, P.; Thoennessen, U. On benchmarking camera calibration and multi-view stereo for high resolution imagery. In Proceedings of the Computer Vision and Pattern Recognition 2008, Anchorage, AK, USA, 23–28 June 2008; pp. 1–8. [[CrossRef](#)]
63. Verhoeven, G. Taking computer vision aloft—Archaeological three-dimensional reconstructions from aerial photographs with PhotoScan. *Archaeol. Prospt.* **2011**, *18*, 67–73. [[CrossRef](#)]
64. Pérez, M.; Agüera, F.; Carvajal, F. Low cost surveying using an unmanned aerial vehicle. *Int. Arch. Photogramm. Remote Sens. Spat. Inf. Sci.* **2013**, *40*, 311–315. [[CrossRef](#)]
65. Gašparović, M.; Gajski, D. Two-step camera calibration method developed for micro UAV's. In Proceedings of the XXIII ISPRS Congress, Prague, Czech Republic, 12–19 July 2016; Volume XLI-b1, pp. 829–833. [[CrossRef](#)]
66. Gašparović, M.; Jurjević, L. Gimbal Influence on the Stability of Exterior Orientation Parameters of UAV Acquired Images. *Sensors* **2017**, *17*, 401. [[CrossRef](#)] [[PubMed](#)]
67. Cardenal, J.; Mata, E.; Perez-Garcia, J.L.; Delgado, J.; Andez, M.; Gonzalez, A.; Diaz-de-Teran, J.R. Close range digital photogrammetry techniques applied to landslide monitoring. *Int. Arch. Photogramm. Remote Sens. Spat. Inf. Sci.* **2008**, *37 Pt B8*, 235–240.
68. Plan Nacional de Ortofotografía Aérea. Available online: <http://pnoa.ign.es/> (accessed on 8 October 2018).
69. González-Díez, A.; Fernández-Maroto, G.; Doughty, M.W.; De Terán, J.D.; Bruschi, V.; Cardenal, J.; Pérez, J.L.; Mata, E.; Delgado, J. Development of a methodological approach for the accurate measurement of slope changes due to landslides, using digital photogrammetry. *Landslides* **2014**, *11*, 615–628. [[CrossRef](#)]
70. Esparza Arroyo, Á. Explotaciones auríferas romanas en el valle del río Negro (Zamora). *Anuario del Instituto de Estudios Zamoranos Florián de Ocampo* **1984**, *1*, 49–54.
71. Domergue, C. Dix-huit ans de recherché (1968–1986) sur les mines d'or romaines du nord-ouest de la Peninsule Iberique. *Actas I Congreso Internacional Astorga Romana* **1986**, *2*, 7–101.
72. Domergue, C.; Sillières, P. *Minas de oro romanas de la provincial de León. I. La Corona de Quintanilla: Excavaciones 1971–1973. Las Coronas de Filiel, Boisan, Luyego 1 y 2: Exploraciones de 1973*; Servicio de Publicaciones del Ministerio de Educación y Ciencia: Madrid, Spain, 1977; p. 183, ISBN 8436902327.
73. Fernández-Lozano, J.; Gutiérrez-Alonso, G. Modelización 3D con tecnología Vant para la reproducción y preservación del registro arqueológico del proyecto de geoparque Las Loras (Palencia-Burgos). In *Investigaciones arqueológicas en el valle del Duero: Del Paleolítico a la Edad Media, Actas de las V Jornadas de Jóvenes Investigadores del valle del Duero*; Glyphos Publicaciones: Valladolid, Spain, 2017; pp. 537–554, ISBN 978-84-946124-0-4.
74. Remondino, F. Heritage recording and 3D modeling with photogrammetry and 3D scanning. *Remote Sens.* **2011**, *3*, 1104–1138. [[CrossRef](#)]
75. Nex, F.; Remondino, F. UAV for 3D mapping applications: A review. *Appl. Geom.* **2014**, *6*, 1–15. [[CrossRef](#)]
76. Shahbazi, M.; Sohn, G.; Théau, J.; Ménard, P. UAV-based point cloud generation for open-pit mine modelling. *Int. Arch. Photogramm. Remote Sens. Spat. Inf. Sci.* **2015**, *40*, 213–320. [[CrossRef](#)]
77. Esposito, G.; Mastrococco, G.; Salvini, R.; Oliveti, M.; Starita, P. Application of UAV photogrammetry for the multi-temporal estimation of surface extent and volumetric excavation in the Sa Pigada Bianca open-pit mine, Sardinia, Italy. *Environ. Earth Sci.* **2017**, *76*, 103. [[CrossRef](#)]
78. Cole, D. Exploring the sustainability of mining heritage tourism. *J. Sustain. Tour.* **2004**, *12*, 480–494. [[CrossRef](#)]
79. Conesa, H.M.; Schulin, R.; Nowack, B. Mining landscape: A cultural tourist opportunity or an environmental problem?: The study case of the Cartagena–La Unión Mining District (SE Spain). *Ecol. Econ.* **2008**, *64*, 690–700. [[CrossRef](#)]
80. Biel-Ibáñez, P. El paisaje minero en España como elemento de desarrollo territorial. Apuntes: Revista de estudios sobre patrimonio cultural. *J. Cult. Herit. Stud.* **2009**, *22*, 6–19.

81. Répola, L.; Memmolo, R.; Signoretti, D. Instruments and methodologies for the underwater tridimensional digitization and data musealization. In Proceedings of the Underwater 3D Recording and Modeling, Piano di Sorrento, Italy, 16–17 April 2015; pp. 183–190. [[CrossRef](#)]
82. Marinos, V.; Vazaios, I.; Papathanassiou, G.; Kaklis, T.; Goula, E. 3D Modelling of the ancient underground quarries of the famous Parian marble in the Aegean Sea, Greece and assessment of their stability using LiDAR scanning. *Q. J. Eng. Geol. Hydrogeol.* **2018**. [[CrossRef](#)]



© 2018 by the authors. Licensee MDPI, Basel, Switzerland. This article is an open access article distributed under the terms and conditions of the Creative Commons Attribution (CC BY) license (<http://creativecommons.org/licenses/by/4.0/>).